Springer

Journal of Mechanical Science and Technology 23 (2009) 2193~2205

Journal of Mechanical Science and Technology

www.springerlink.com/content/1738-494x
DOI 10.1007/s12206-009-0515-0

Effects of nearfield waves and phase information on the vibration analysis of curved beams †

Cheol-Ho Jeong[1] and Jeong-Guon Ih[2,*]

[1]*Acoustic Technology, Department of Electrical Engineering, Technical University of Denmark, DK-2800 Kgs. Lyngby, Denmark*
[2]*Center for Noise and Vibration Control (NoViC), Department of Mechanical Engineering, KAIST, Daejeon 305-701, Korea*

(Manuscript Received January 15, 2009; Revised March 23, 2009; Accepted March 26, 2009)

Abstract

At high frequencies, energy methods such as the statistical energy analysis and the power flow analysis have been popularly used to predict the averaged responses of vibro-acoustic subsystems. Usually, these energy methods ignore flexural nearfield components and phase information, mainly for simplicity. Such assumptions sometimes lead to an erroneous conclusion, in particular for complex structures and at medium frequencies around the Schroeder cutoff frequency. This paper deals with the effects of nearfield waves and phase information at medium to high frequencies by using the ray tracing method (RTM). A curved beam and a coupled beam system were chosen as test examples, which exhibit the typical mode conversion between various types of travelling waves. Propagation of longitudinal, flexural, and torsional waves was studied based on the Euler-Bernoulli beam theory. Analyses of the spatial distribution of vibrational energy quantities revealed that the conventional RTM could mimic the overall trend of the traveling wave solution. However, the results varied smoothly in space due to the neglect of wave interference. By considering the phase information, local fluctuations of vibration energy could be correctly described. It was confirmed that the flexural nearfield plays a significant role near boundaries and junctions. It was also shown that the accuracy of the analysis depends mainly on the modal overlap factor. Similar to other high frequency methods, the results become close to the traveling wave solutions as the modal overlap factor increases.

Keywords: Curved beams; High frequency energy method; Nearfield waves; Phase information; Ray tracing method

1. Introduction

In the vibro-acoustic design of structures, wave based methods such as the finite element method and the boundary element method are effective for low frequency prediction. However, it is well known that these methods are not suitable for mid-to-high frequency analyses because of errors due to a small mesh size, huge number of elements, high order interpolation functions, and excessive modal overlap. At high frequency bands, where modes are highly overlapped, the statistical energy analysis (SEA) has been widely used to predict time-, frequency-, and space-averaged responses of built-up structures [1]. Applications of the SEA are limited by many underlying assumptions and the fact that results do not provide detailed information, viz., spatial distributions of vibration responses in a subsystem of a complex structure. To predict how vibration energy distributes, the power flow analysis (PFA) has been suggested [2, 3]. The PFA can predict frequency-averaged vibrational behavior of a structure in much the same manner as the SEA. However, it was shown that the two-dimensional PFA would be valid only for structures having a relatively small damping factor or highly reverberant wave field [4]. Le Bot also pointed out that a small damping loss factor is required for applications of the PFA [5].

† This paper was recommended for publication in revised form by Associate Editor Yeon June Kang
* Corresponding author. Tel.: +82 42 350 3035, Fax.: +82 42 350 8211
E-mail address: J.G.IH@kasit.ac.kr

The ray tracing method (RTM) has been popularly adopted in the architectural acoustics area to predict acoustic impulse responses and field distributions at high frequencies [6, 7]. Initially, sound rays are emanated from an excitation point and their propagating paths are traced. A response at an observation point is obtained by accumulating all contributions of sound rays. Basic applications of the RTM to the structure-borne wave propagation have already been proposed [8], but it is rare to see literatures that deal with a detailed technique in applying it to specific structures.

There are a number of curved structural elements that constitute real structures such as bridges, ships, vehicles, aircrafts, etc. For effective noise control, it is felt that considerable effort should be focused on accurate modeling of vibrational energy flow. In this paper, as an incipient attempt for this purpose, high frequency energy transmission through a curved beam was studied for the prediction of energy distribution in space. Energy reflection and transmission in a single curved beam and a two-beam connected curved structure were modeled and analyzed by using the RTM including actions of longitudinal, flexural, and torsional waves. The ultimate purpose of the paper is to shed light on the effects of nearfield wave terms and phase information in analyzing beam vibrations.

2. Kinetic model of the curved beam

The curvature of a beam leads to a variety of shapes, which significantly modifies the vibrational behavior of the beam. A peculiar characteristic of curved structures is that the structure deforms simultaneously in more than two independent coordinates by a single wave excitation. Four important wave modes are conveyed in an elastic beam: a longitudinal wave, a torsional wave, and flexural waves in two directions. Previous studies are categorized into two groups: One group has studied the coupling between the longitudinal wave and one flexural wave [5, 9-11], and others have focused on the coupling between the torsion and the other type of flexural wave [12-18], mostly by civil engineers. However, research works on the coupling among four wave types are rather scanty so far [19, 20].

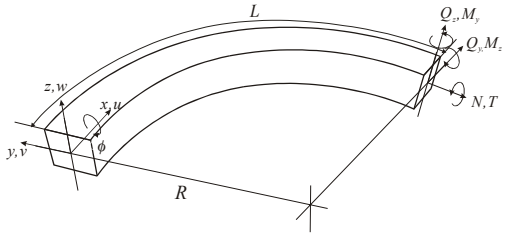

Fig. 1. Definitions of geometry and coordinate system of a curved beam.

Governing equations of a curved beam have been given by Love [21], Morley [22], and Vlasov [23]. The dynamic equations of the harmonic motion of a curved beam based on the Euler-Bernoulli theory can be expressed as follows (see Fig. 1):

$$\frac{EI_z}{R}\frac{d^2}{dx^2}\left(\frac{u}{R}-\frac{dv}{dx}\right)+ES\frac{d}{dx}\left(\frac{du}{dx}+\frac{v}{R}\right)=-\rho S\omega^2 u,$$

$$EI_z\frac{d^3}{dx^3}\left(\frac{u}{R}-\frac{dv}{dx}\right)-\frac{ES}{R}\left(\frac{du}{dx}+\frac{v}{R}\right)=-\rho S\omega^2 v,$$

$$-EI_y\frac{d^4w}{dx^4}+\frac{GJ}{R^2}\frac{d^2w}{dx^2}+\frac{EI_y+GJ}{R}\frac{d^2\phi}{dx^2}=-\rho S\omega^2 w,$$

$$GJ\frac{d^2\phi}{dx^2}-\frac{EI_y}{R^2}\phi+\frac{EI_y+GJ}{R}\frac{d^2w}{dx^2}=-\rho I_p\omega^2\phi. \quad \text{(1a-d)}$$

Here, u denotes the normal displacement along the axial direction x, v and w are the displacements in the direction of y and z axes, respectively, ϕ the rotation angle about the axial axis x, E and G the complex elastic and shear moduli, respectively, ρ the mass density, I_p the polar moment of inertia of the section, S the cross sectional area, I_y and I_z the principal moment of inertias of the section, J the torsional constant, ω the angular frequency of the harmonic motion, and R the radius of curvature.

The Euler-Bernoulli theory basically assumes negligible flexural rotary inertia and shear deformation. In the present study, uniform cross-section and constant radius of curvature are assumed, and warping is also neglected. The equations governing the behavior of axial deformation and flexural deformation along the y-axis are coupled in terms of u and v. Similarly, the equations describing beam flexure about the z-axis and torsion are coupled in terms of w and ϕ. Propagation characteristics are obtained by assuming harmonic waves in the form of

$$u(x,t)=u_o e^{-j(kx-\omega t)},\ v(x,t)=v_o e^{-j(kx-\omega t)},$$
$$w(x,t)=w_o e^{-j(kx-\omega t)},\ \phi(x,t)=\phi_o e^{-j(kx-\omega t)}. \quad \text{(2a-d)}$$

A non-dimensionalized form of the governing equation is given by

$$\begin{bmatrix} \left(\frac{\Omega^2}{r_z^2}-\frac{K^2}{r_z^2}-K^2\right) & -j\left(\frac{K^3}{r_z}+\frac{K}{r_z}\right) & 0 & 0 \\ j\left(\frac{K^3}{r_z}+\frac{K}{r_z}\right) & \left(\frac{\Omega^2}{r_z^2}-\frac{K^4}{r_z^2}-1\right) & 0 & 0 \\ 0 & 0 & \left(\frac{\Omega^2}{r_z^2}-\frac{K^4}{a^2r_z^2}-\frac{K^2}{\mu^2}\right) & -\left(\frac{K^2}{a^2}+\frac{K^2}{\mu^2}\right) \\ 0 & 0 & -\left(\frac{K^2}{a^2}+\frac{K^2}{\mu^2}\right) & \left(\frac{\Omega^2}{b^2}-\frac{K^2}{\mu^2}-\frac{r_z^2}{a^2}\right) \end{bmatrix} \begin{Bmatrix} u_o \\ v_o \\ w_o \\ R\phi_o \end{Bmatrix} = \begin{Bmatrix} 0 \\ 0 \\ 0 \\ 0 \end{Bmatrix} \tag{3}$$

where $\Omega = \omega\kappa_z / c_l''$ denotes the non-dimensional frequency, $K = \kappa_z k$ the non-dimensional wave number, $a = \kappa_z / \kappa_y$ and $b = \kappa_z / \kappa_p$ the non-dimensional radii of gyration, $r_z = \kappa_z / R$ the non-dimensional radius of curvature, $\mu = \kappa_z / \alpha$ the non-dimensional stiffness ratio, $c_l'' = \sqrt{E/\rho}$ the longitudinal wave speed in a bar, κ_y, κ_z, κ_p the radii of gyration for I_y, I_z, I_p, respectively, such that $\kappa_y = \sqrt{I_y / S}$, $\kappa_z = \sqrt{I_z / S}$, $\kappa_p = \sqrt{I_p / S}$, and $\alpha = \sqrt{GJ / ES}$ the ratio of torsional stiffness to longitudinal stiffness.

Freely propagating harmonic waves may exist only if the determinant in the above system vanishes. The resulting dispersion equation is given by

$$c_{12}K^{12} + c_{10}K^{10} + c_8K^8 + c_6K^6 + c_4K^4 + c_2K^2 + c_o = 0, \tag{4}$$

where

$$\begin{aligned} c_{12} &= \left(\frac{1}{a^2\mu^2r_z^6}+\frac{1}{a^2\mu^2r_z^4}\right), \quad c_{10} = \left(-\frac{\Omega^2}{a^2b^2r_z^6}-\frac{\Omega^2}{a^2b^2r_z^4}-\frac{\Omega^2}{a^2\mu^2r_z^6}+\frac{1}{a^4r_z^4}+\frac{1}{\mu^4r_z^4}-\frac{2}{a^2\mu^2r_z^2}\right), \\ c_8 &= \left(\begin{array}{l}\frac{\Omega^4}{a^2b^2r_z^6}-\frac{\Omega^2}{\mu^2r_z^6}-\frac{\Omega^2}{a^2\mu^2r_z^6}-\frac{\Omega^2}{a^2r_z^4}-\frac{\Omega^2}{\mu^4r_z^4}-\frac{\Omega^2}{\mu^2r_z^4}-\frac{\Omega^2}{a^2\mu^2r_z^4}-\frac{\Omega^2}{b^2\mu^2r_z^2} \\ +\frac{1}{a^2\mu^2r_z^4}+\frac{1}{a^2\mu^2}-\frac{2}{a^4r_z^2}-\frac{2}{\mu^4r_z^2}-\frac{2}{a^2\mu^2r_z^2}-\frac{2}{b^2\mu^2r_z^2}\end{array}\right), \\ c_6 &= \left(\begin{array}{l}\frac{\Omega^4}{b^2r_z^6}+\frac{\Omega^4}{a^2b^2r_z^6}+\frac{\Omega^4}{\mu^2r_z^6}+\frac{\Omega^4}{a^2\mu^2r_z^6}+\frac{\Omega^4}{a^2b^2r_z^4}+\frac{\Omega^4}{b^2\mu^2r_z^4}+\frac{\Omega^4}{b^2r_z^4} \\ -\frac{\Omega^2}{a^4r_z^4}-\frac{\Omega^2}{a^2r_z^4}-\frac{\Omega^2}{a^2b^2r_z^4}-\frac{\Omega^2}{\mu^4r_z^4}-\frac{\Omega^2}{a^2\mu^2r_z^4}-\frac{\Omega^2}{a^4r_z^2}-\frac{\Omega^2}{a^2r_z^2}-\frac{\Omega^2}{a^2b^2r_z^2}-\frac{\Omega^2}{\mu^4r_z^2}-\frac{\Omega^2}{a^2\mu^2r_z^2} \\ +\frac{1}{a^4}+\frac{1}{\mu^4}-\frac{2}{a^2\mu^2r_z^2}\end{array}\right), \\ c_4 &= \left(\begin{array}{l}-\frac{\Omega^6}{b^2r_z^6}-\frac{\Omega^6}{a^2b^2r_z^6}+\frac{\Omega^4}{b^2\mu^2r_z^2}+\frac{\Omega^4}{\mu^2r_z^6}+\frac{\Omega^4}{a^4r_z^4}+\frac{\Omega^4}{a^2r_z^4}+\frac{\Omega^4}{a^2b^2r_z^4}+\frac{\Omega^4}{\mu^4r_z^4}+\frac{\Omega^4}{\mu^2r_z^4}+\frac{\Omega^4}{b^2\mu^2r_z^4} \\ -\frac{\Omega^2}{a^4r_z^2}-\frac{\Omega^2}{\mu^4r_z^2}-\frac{\Omega^2}{\mu^2r_z^2}-\frac{\Omega^2}{a^2\mu^2r_z^2}-\frac{\Omega^2}{b^2\mu^2r_z^2}-\frac{\Omega^2}{\mu^2r_z^4}-\frac{\Omega^2}{a^2\mu^2}+\frac{1}{a^2\mu^2}+\frac{r_z^2}{a^2\mu^2}\end{array}\right), \\ c_2 &= \left(\begin{array}{l}-\frac{\Omega^6}{b^2r_z^6}-\frac{\Omega^6}{\mu^2r_z^6}-\frac{\Omega^6}{b^2r_z^4}-\frac{\Omega^6}{b^2\mu^2r_z^4} \\ +\frac{\Omega^4}{a^2r_z^4}+\frac{\Omega^4}{b^2r_z^4}+\frac{\Omega^4}{\mu^2r_z^4}+\frac{\Omega^4}{a^2r_z^2}+\frac{\Omega^4}{b^2r_z^2}+\frac{\Omega^4}{a^2\mu^2r_z^2}+\frac{\Omega^4}{b^2\mu^2r_z^2}-\frac{\Omega^2}{a^2r_z^2}-\frac{\Omega^2}{a^2}-\frac{\Omega^2}{a^2\mu^2}\end{array}\right), \\ c_0 &= \left(\frac{\Omega^8}{b^2r_z^6}-\frac{\Omega^6}{a^2r_z^4}-\frac{\Omega^6}{b^2r_z^4}+\frac{\Omega^4}{a^2r_z^2}\right). \end{aligned} \tag{5}$$

Because Eq. (4) is an even function, six pairs of roots are found. Each pair has the same amplitude with opposite signs, which means the two traveling waves propagating in opposite directions. The wave number are generally complex valued as

$$\begin{aligned} &k_l, -k_l, k_{fy}^p, -k_{fy}^p, k_{fy}^e, -k_{fy}^e, \\ &k_{fz}^p, -k_{fz}^p, k_{fz}^e, -k_{fz}^e, k_t, -k_t, \end{aligned} \tag{6}$$

where the subscript l refers to the longitudinal waves, fy to the flexural waves in the y-direction, fz to the flexural waves in the z-direction, t to the torsional waves, and the superscript p denotes the propagating waves, and e the evanescent components. As can be seen, there are four nearfield wave components. Therefore, displacement variables, having six terms for each, can be expressed as

$$\begin{aligned} u(x,t) &= \sum_{i=1}^{3}\left[u_i^+ e^{-j(k_i x-\omega t)} + u_i^- e^{j(k_i x-\omega t)}\right], \\ v(x,t) &= \sum_{i=1}^{3}\left[v_i^+ e^{-j(k_i x-\omega t)} + v_i^- e^{j(k_i x-\omega t)}\right], \\ \phi(x,t) &= \sum_{i=1}^{3}\left[\phi_i^+ e^{-j(k_i x-\omega t)} + \phi_i^- e^{j(k_i x-\omega t)}\right], \\ w(x,t) &= \sum_{i=1}^{3}\left[w_i^+ e^{-j(k_i x-\omega t)} + w_i^- e^{j(k_i x-\omega t)}\right]. \end{aligned} \tag{7a-d}$$

In these solutions, the coupling between u and v is expressed by the relation as follows:

$$v_i^+ / u_i^+ = -v_i^- / u_i^- = -j\left(\frac{K^3}{r_z}+\frac{K}{r_z}\right) / \left(\frac{\Omega^2}{r_z^2}-\frac{K^4}{r_z^2}-1\right). \tag{8}$$

Here, the superscript + or – denotes the positively or the negatively propagating component, respectively. Similarly, the coupling between ϕ and w can be expressed as

$$\phi_i^+ / w_i^+ = \phi_i^- / w_i^- = \left(\frac{K^2}{a^2}+\frac{K^2}{\mu^2}\right) / R \cdot \left(\frac{\Omega^2}{b^2}-\frac{K^2}{\mu^2}-\frac{r_z^2}{a^2}\right). \tag{9}$$

Resultant forces in the curved beam are defined as

$$\begin{aligned} &N = ES\left(\frac{du}{dx}+\frac{v}{R}\right), T = GJ\left(\frac{d\phi}{dx}+\frac{1}{R}\frac{dw}{dx}\right), \\ &Q_y = EI_z\left(\frac{1}{R}\frac{d^2u}{dx^2}-\frac{d^3v}{dx^3}\right), Q_z = EI_y\left(\frac{1}{R}\frac{d\phi}{dx}-\frac{d^3w}{dx^3}\right), \\ &M_y = EI_y\left(\frac{\phi}{R}-\frac{d^2w}{dx^2}\right), M_z = EI_z\left(\frac{1}{R}\frac{du}{dx}-\frac{d^2v}{dx^2}\right). \end{aligned} \tag{10a-f}$$

Then, the total energy density e and the power flow I for each wave component are given by the following equations:

$$e_l(x)=\frac{\rho S\omega^2}{4}uu^*+\frac{ES}{4}\left(\frac{v}{R}+\frac{du}{dx}\right)\left(\frac{v}{R}+\frac{du}{dx}\right)^*,$$

$$e_t(x)=\frac{\rho I_p\omega^2}{4}\phi\phi^*+\frac{GJ}{4}\left(\frac{d\phi}{dx}+\frac{1}{R}\frac{dw}{dx}\right)\left(\frac{d\phi}{dx}+\frac{1}{R}\frac{dw}{dx}\right)^*,$$

$$e_{fy}(x)=\frac{\rho S\omega^2}{4}vv^*+\frac{EI_z}{4}\frac{d}{dx}\left(\frac{u}{R}-\frac{dv}{dx}\right)\frac{d}{ds}\left(\frac{u}{R}-\frac{dv}{dx}\right)^*,$$

$$e_{fz}(x)=\frac{\rho S\omega^2}{4}ww^*+\frac{EI_y}{4}\left(\frac{\phi}{R}-\frac{d^2w}{dx^2}\right)\left(\frac{\phi}{R}-\frac{d^2w}{dx^2}\right)^*, \quad (11a\text{-}d)$$

$$I_l=\mathrm{Real}\left(\frac{j\omega}{2}\left\{N+\frac{M_z}{R}\right\}u^*\right),$$

$$I_t=\mathrm{Real}\left(\frac{j\omega}{2}\left\{T\phi^*+\frac{M_y}{R}w^*\right\}\right),$$

$$I_{fy}=\mathrm{Real}\left(\frac{j\omega}{2}\left\{Q_y v^*-M_z\frac{dv^*}{ds}\right\}\right), \quad (12a\text{-}d)$$

$$I_{fz}=\mathrm{Real}\left(\frac{j\omega}{2}\left\{Q_z w^*-M_y\frac{dw^*}{ds}\right\}\right).$$

3. The ray tracing method

3.1 Basic concept of RTM for structural acoustics

The ray tracing method, stemming from optics, is one of the geometrical acoustic simulation techniques, which has been widely applied to various acoustic areas, such as room acoustics, environmental acoustics, geophysics, underwater acoustics, etc. In applying the RTM, a sound source is modeled by a large number of sound rays, which are projected into a target field in a very narrow and even angular spacing. A ray is basically an infinitesimally thin line, which travels perpendicular to the surface of constant phase. Plane wave propagation in a beam structure can be replaced by a ray traveling along the axial direction, because the wavefront is always perpendicular to the axial coordinate of beams. Because energies are only carried by rays without phase information, the RTM is reliable only if the beam length L is much longer than the wavelength λ [24].

Several attempts have been made to analyze the structures by using the geometrical acoustics concept. Gunda et al. [25] applied the image source method (ISM) to a flat plate. The ISM utilizes mirror image sources outside of a real structure to satisfy boundary conditions. Parot and Thirard [26] analyzed a truss structure and a coupled plate by using the RTM. Chae and Ih [8] studied the applicability of RTM to a flat plate and a coupled structure, in which results were compared with those of the modal summation method and other high frequency methods.

When a beam structure is excited, initial waves are generated from the excitation point as depicted in Fig 2(a). The magnitude and phase of the initial waves are determined by the continuity equations of forces and moments at the excitation point. Propagation of initial waves can be regarded as a direct field or a response of the corresponding infinite structure. When the initial waves encounter the boundaries, reflected waves are generated; after a sufficient number of reflections, the steady state response reaches a converged value. Finally, the total response at an observation point is comprised of the direct field and the reflected field as follows:

$$w(\vec{x}_o,\vec{x}_s;\omega)=w_{dir}(\vec{x}_o,\vec{x}_s;\omega)+\sum_{n=1}^{\infty}w_{refl,n}(\vec{x}_o,\vec{x}_{\partial\Omega};\omega). \quad (13)$$

Similarly, the impulse response for a source-receiver pair is expressed as follows:

$$h(\vec{x}_o,\vec{x}_s;t)=h_\infty(\vec{x}_o,\vec{x}_s;t)+h_{refl}(\vec{x}_o,\vec{x}_s;t). \quad (14)$$

where x_o and x_s mean the observation point and excitation point, respectively. The first term is the impulse response of an infinite structural element $h_\infty(\vec{x}_o,\vec{x}_s;t)$. Successive signals arriving at the observation point can be represented by the reflected wave field $h_{refl}(\vec{x}_o,\vec{x}_s;t)$.

Generally, high frequency results can be expressed in terms of energy quantities. Quadratic responses of the wave field parameter, e.g., displacement or velocity, can be derived as

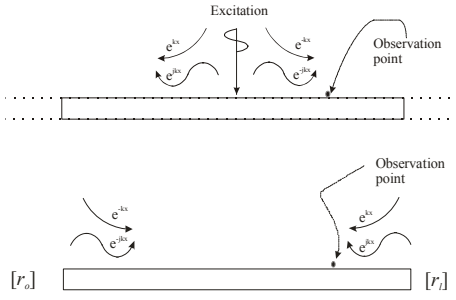

Fig. 2. Schematic drawing of the ray tracing method for one-dimensional system: (a) direct field, (b) reflected field. [r_o] and [r_1] denote the reflection coefficient matrices at x=0 and x=l, respectively.

$$\begin{aligned}\left|w(\vec{x}_o,\vec{x}_s;\omega)\right|^2 &= \left|w_{dir}(\vec{x}_o,\vec{x}_s;\omega)\right|^2 \\ &+ \sum_{n=1}^{\infty}\left|w_{refl}(\vec{x}_o,\vec{x}_s;\omega)_n\right|^2 \\ &+2\,\mathrm{Re}\left\{w_{dir}(\vec{x}_o,\vec{x}_s;\omega)\sum_{n=1}^{\infty}w^*_{refl}(\vec{x}_o,\vec{x}_s;\omega)_n\right\} \\ &+2\,\mathrm{Re}\left\{\sum_{n=1}^{\infty}\sum_{m=1,m\neq n}^{\infty}w_{refl}(\vec{x}_o,\vec{x}_s;\omega)_n\,w^*_{refl}(\vec{x}_o,\vec{x}_s;\omega)_m\right\}.\end{aligned} \tag{15}$$

In Eq. (15), the first and second terms on the right hand side represent the exponentially varying (exponentially decreasing in most cases) fields. The last two terms mean the interaction between the direct and the reflected waves and the interferences between the reflected waves. These have a spatially fluctuating characteristic and can be smoothed out throughout a frequency band integration.

Although reflected waves from boundaries are originated from the direct wave, they have different phase characteristic determined by the boundary conditions. After several reflections, the reflected phase becomes random and incoherent with that of the direct sound, particularly at high frequencies. Conducting a frequency band integration of Eq. (15) under the assumption of the presence of several modes within the band, the response fluctuation due to the interference terms could be flattened out as

$$\begin{aligned}&\int_{\omega_1}^{\omega_2}\left|w(\vec{x}_o,\vec{x}_s;\omega)\right|^2 d\omega \cong \\ &\int_{\omega_1}^{\omega_2}\left|w_{dir}(\vec{x}_o,\vec{x}_s;\omega)\right|^2 d\omega+\sum_{n=1}^{\infty}\int_{\omega_1}^{\omega_2}\left|w_{refl}(\vec{x}_o,\vec{x}_s;\omega)_n\right|^2 d\omega.\end{aligned} \tag{16}$$

Once the quadratic response is determined as Eq. (16), all energy quantities including energy densities and power flows in each band can be calculated according to Eqs. (11) and (12).

3.2 Field transfer matrix

The first step in applying the RTM to a curved beam structure is to calculate the wave numbers based on Eq. (4). Roots of the dispersion equation, Eq. (4), become close to those of a straight beam, if the radius of curvature goes infinite or the frequency increases. Using the calculated wave numbers, a field transfer matrix can be constructed. Eq. (17) shows an example of the transfer matrix for only positively propagating waves. It should be noted that two evanescent flexural waves are included as the 3rd and the 6th diagonal components. Above the ring frequency, waves in beams are supposed to have the following properties [27]: (i) predominantly longitudinal traveling wave; (ii) predominantly torsional traveling wave; (iii) predominantly flexural traveling wave along *y*-direction; (iv) predominantly flexural traveling wave along *z*-direction; (v) predominantly flexural nearfield wave along *y*-direction; and (vi) predominantly flexural nearfield wave along *z*-direction.

$$[T_d]_s=\begin{bmatrix} e^{-jk_l s} & 0 & 0 & 0 & 0 & 0 \\ 0 & e^{-jk^p_{fy}s} & 0 & 0 & 0 & 0 \\ 0 & 0 & e^{-jk^e_{fy}s} & 0 & 0 & 0 \\ 0 & 0 & 0 & e^{-jk_t s} & 0 & 0 \\ 0 & 0 & 0 & 0 & e^{-jk^p_{fz}s} & 0 \\ 0 & 0 & 0 & 0 & 0 & e^{-jk^e_{fz}s} \end{bmatrix}. \tag{17}$$

Here, j denotes the imaginary unit ($=\sqrt{-1}$), η the structural loss factor, and s the propagation distance from the reference point. All components in the matrix are complex valued. A diagonal transfer matrix means that a wave type does not couple with the other wave types during propagation. Mode conversion can occur only at boundaries. A field transfer function for energy quantities is obtained by squaring Eq. (17):

$$[T_e]_s=\begin{bmatrix} e^{-2\mathrm{Im}(k_l)s} & 0 & 0 & 0 & 0 & 0 \\ 0 & e^{-2\mathrm{Im}(k^p_{fy})s} & 0 & 0 & 0 & 0 \\ 0 & 0 & e^{-2\mathrm{Im}(k^e_{fy})s} & 0 & 0 & 0 \\ 0 & 0 & 0 & e^{-2\mathrm{Im}(k_t)s} & 0 & 0 \\ 0 & 0 & 0 & 0 & e^{-2\mathrm{Im}(k^p_{fz})s} & 0 \\ 0 & 0 & 0 & 0 & 0 & e^{-2\mathrm{Im}(k^e_{fz})s} \end{bmatrix}. \tag{18}$$

Obviously, vibrational energy quantities decay exponentially as waves travel. Assuming a hysteresis damping, a complex elastic modulus $E_o(1+j\eta)$ is introduced instead of an elastic modulus E_o. A complex wavenumber is given by $k=k_o-j\omega\eta/2c_g$ for all waves. Here, k_o is the wavenumber in a lossless medium and c_g the group velocity. Consequently the exponent $-2\mathrm{Im}(k)$ is given by $\omega\eta/c_g$, which is the propagation property in the PFA [5]. Note that the energy decay characteristics for all waves are expressed in the same manner, although the group velocity of the flexural

wave is twice the phase velocity, being different from other waves. It is noted that in the conventional ray tracing method, flexural evanescent waves are not considered. By ignoring two nearfield components, only four types of waves can exist: (i) predominantly longitudinal traveling wave; (ii) predominantly torsional traveling wave; (iii) predominantly flexural traveling wave along *y*-direction; and (iv) predominantly flexural traveling wave along *z*-direction.

3.3 Calculation of reflection/transmission coefficients

A correct description of boundary and coupling conditions is crucial for the precision of the RTM. The nature of coupling between neighboring structures and boundary conditions can be expressed in terms of the reflection and transmission coefficients, which are obtained by continuity equations of displacements, rotations, forces, and moments. During the calculation of coefficients, beams are assumed to be semi-infinite in the direction of departing from the junction, at which one wants to determine the coefficients. A semi-infinite structure ensures that there is no wave returning back from the other boundary.

In Fig. 3, there are two boundaries and one junction for a coupled beam system. At the boundaries, six types of reflected waves are generated by an incident wave. Therefore, one should have six continuity equations in order to compute six reflection coefficients. For example, to satisfy the free boundary condition at x=0, forces and moments should vanish as follows:

$$N(0) = ES\left(\frac{du(0)}{dx} + \frac{v(0)}{R}\right) = 0,$$

$$T(0) = GJ\left(\frac{d\phi(0)}{dx} + \frac{1}{R}\frac{dw(0)}{dx}\right) = 0,$$

$$Q_y(0) = EI_z\left(\frac{1}{R}\frac{d^2u(0)}{dx^2} - \frac{d^3v(0)}{dx^3}\right) = 0, \quad \text{(19a-f)}$$

$$Q_z(0) = EI_y\left(\frac{1}{R}\frac{d\phi(0)}{dx} - \frac{d^3w(0)}{dx^3}\right) = 0,$$

$$M_y(0) = EI_y\left(\frac{\phi(0)}{R} - \frac{d^2w(0)}{dx^2}\right) = 0,$$

$$M_z(0) = EI_z\left(\frac{1}{R}\frac{du(0)}{dx} - \frac{d^2v(0)}{dx^2}\right) = 0.$$

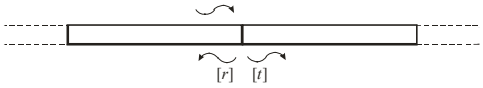

Fig. 3. A coupled beam model. Reflection coefficients [*r*] and transmission coefficients [*t*] are calculated by assuming semi-infinite beams.

Similarly, for the clamped boundary condition, displacements (u, v, w) and rotations along x and y and z-direction should vanish. At the coupled junction, displacements, rotations, forces, and moments should have the same value at the right end of the left beam and at the left end of the right beam. Twelve continuity equations end up with six reflected and six transmitted coefficients, which clearly indicate the wave conversion phenomenon at the coupled junction. Wu and Lundberg [27] also adopted the same method for elastic longitudinal and flexural waves in a bent bar.

Magnitudes of the reflection and transmission coefficients should not exceed unity in accordance with the energy conservation principle. For estimating energy quantities, power reflection and transmission coefficients can be obtained by squaring the pressure reflection and transmission coefficients. One can expect that nearfield terms get significant near the discontinuities. However, because the evanescent waves diminish very quickly in the vicinity of boundaries or junctions, nearfield terms have been commonly neglected for energy methods [28]. However, the effects of nearfield components will be discussed in the next section.

3.4 Valid condition for high frequency analyses

In general, the validity of high frequency methods is based on two parameters: a modal overlap factor and a mode count in a band. Fahy and Mohammed [29] concluded that two parameters controlling the variability of power flow are the modal overlap factor (MOF=$\eta\omega n$ (ω); n (ω) being the modal density) of an uncoupled subsystems and the number of coupled modes of a total system. The coupling loss factor was found to exceed the actual value when the average MOF is much less than unity. According to their research, it is necessary to have at lease five modes in a band or the modal overlap factor should exceed unity. Moens et al. [30] suggested a wavelength criterion for the PFA based on analyses by Morley [21]. They conducted a numerical validation for plates and coupled plates by changing the hysteretic damping.

Because the RTM utilizes the free-space Green function of an infinite structure, the accuracy of RTM is affected by the energy ratio of the direct field to the reflected field; when the damping is high enough, the direct field becomes dominant compared to the reflected field. Hence the RTM can yield far accurate result than in small damping cases. In sufficiently long beams, one could imagine that the energy ratio

gets high. Considering these two conditions, the MOF might be more appropriate parameter than the mode count for the RTM. Recall that the Schroeder cutoff frequency [28], which discriminates between high and low frequency range, is also affected by the equivalent absorption area, which is the multiplication of the total area (dimensions) and the average damping. The modal densities for longitudinal, flexural, and torsional waves in beams are given by

$$\begin{aligned} n_l(\omega) &= L/c_l^{"}\pi, \\ n_f(\omega) &= L/3.4\sqrt{c_l^{"}h\omega}, \\ n_t(\omega) &= L/c_t\pi. \end{aligned} \qquad \text{(20a-c)}$$

Thus, the MOF is directly proportional to the frequency for longitudinal and torsional waves, not for flexural waves. The MOF increases with the loss factor and the length of beams.

4. Numerical simulation

Spectral analyses using energy methods are commonly conducted based on 1/3 or 1/1 octave band at high frequencies. In estimating energy responses, non-propagating components and the interference effects among propagating waves have been generally neglected. However, in this study two comparisons are emphasized: the effect of non-propagating components near boundaries and junctions, and the effect of interferences. To do so, the RTM was modified considering the phase information. Then the method could predict displacement responses according to Eqs. (14) and (17), which employed pressure reflection and transmission coefficients from semi-infinite structures, as described in Section 3.3. Similar works have been conducted for 3-dimenstional room acoustic simulations by the authors [31, 32].

A typical single curved beam model is illustrated in Fig. 1. Material and dimensional data of the curved beam under consideration are as follows: mass density ρ=7800 kg/m^3, Young's modulus E=210 GPa (steel), width b=1×10^{-2} m, thickness h=1×10^{-2} m, length L=1 m, and radius of curvature R=0.25 m. RTM results were compared to solutions of the traveling wave method (TWM), which is regarded as the exact solution.

First, a displacement distribution was simulated by a modified RTM considering phase. Note that evanescent wave components were also included in the analysis. Figure 4 shows spatial distributions of displacements for a pure tone excitation at 100 Hz with η=0.005, low damping case. Obviously, such a condition is not favorable for high frequency energy methods. The two boundaries were modeled as a free-free condition and excitation forces were exerted at the right end as $\{N, Q_y, Q_z, M_y, M_z, T\}$={1,1,1,1,1,1}. The predicted displacements for a 100 Hz pure tone excitation agrees well with the TWM solution.

In Fig. 4(a), one can find that longitudinal waves are traveling even below the ring frequency of 3.3 kHz, which might be contradictory to the general notion that the longitudinal wave cannot propagate below the ring frequency. However, it is true that the evanescent waves can propagate when the distance between neighboring discontinuities is short. In our

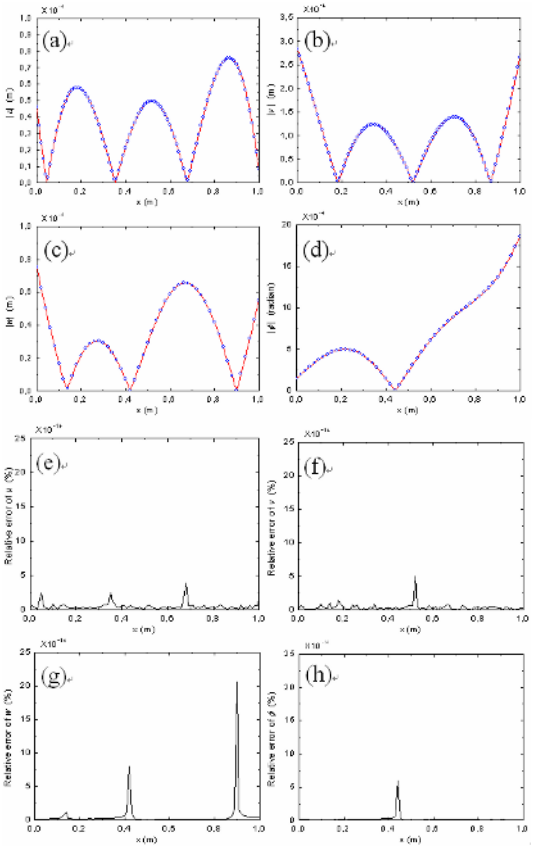

Fig. 4. Spatial distributions of displacements for a pure tone excitation at 100 Hz with η=0.005: (a) longitudinal displacement; (b) flexural displacement in y coordinate; (c) flexural displacement in z coordinate; (d) rotation angle; (e) error of longitudinal displacement; (f) error of flexural displacement in y direction; (g) error of flexural displacement in z direction; (h) error of rotation angle. ———, TWM; ○, modified RTM considering phase and evanescent waves.

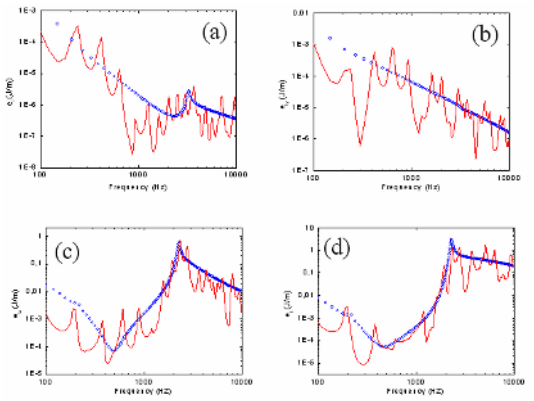

Fig. 5. Frequency responses of energy densities at x=0.3 m with η=0.05; (a) longitudinal energy density; (b) flexural energy density in y direction; (c) flexural energy density in z direction; (d) torsional energy density. ———, TWM; ○, conventional RTM.

case, the curved beam can be considered as a continuous discontinuity in its sectional area and the normal direction of it. Also, one can find that, according to Ref. 11, the calculation frequency of 100 Hz belongs to the region II of the reference paper, where two predominant flexural waves and four decaying oscillating waves co-exist. This example clearly proves the capability of the modified ray model considering phase and evanescent waves for one-dimensional structure.

Fig. 5 shows frequency responses of energy density using the conventional ray model at an observation point at x=0.3 m. The conventional RTM solution neglecting both nearfield waves and interference can represent the tendency of the exact solution. At low frequencies and for low MOF, the predicted frequency response is somewhat overestimated. In the longitudinal energy density analysis in Fig. 5(a), a single peak appears at the ring frequency of 3.3 kHz. Predicted spatial distributions of energy density and power flow are displayed in Fig. 6. The frequency range of interest is an octave band centered at 8 kHz with the damping loss factor of η=0.05.

One can notice that it is a rather favorable condition for high frequency energy methods. The RTM solution shows a spatially smooth curve without local oscillation, but the tendency is well predicted. It can be interpreted that the conventional RTM is capable of predicting an overall trend of energy densities and power flows in space.

In Fig. 6, the energy density of the right side of the curved beam is relatively high and consequently the

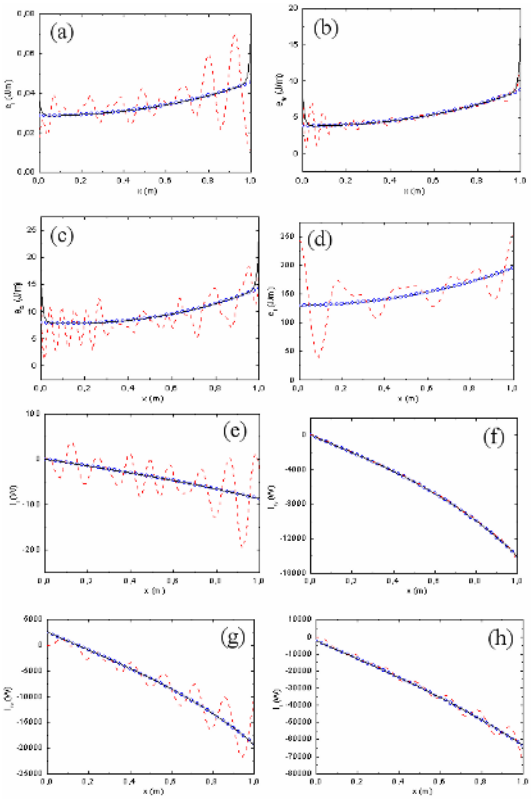

Fig. 6. Spatial distributions of energies for the beam excited at right end (8 kHz octave band; η=0.05): (a) longitudinal energy density; (b) flexural energy density in y direction; (c) flexural energy density in z direction; (d) torsional energy density, (e) longitudinal energy power flow; (f) flexural power flow in y direction; (g) flexural power flow in z direction; (h) torsional power flow. – – –, TWM; ○, conventional RTM; ———, RTM considering evanescent wave.

power flows in the negative direction. It is expected that all the active power flows at the left end should vanish theoretically, but the results of the RTM differ, particularly in Figs 6(g) and 6(h).

However, the sum of the longitudinal and the flexural power flows at x=0 in Figs. 6(e) and 6(f) and the sum of the other two power flows in Figs. 6(g) and 6(h) become exactly zero at x=0. It is an apparent evidence of energy conversion happening in the ray model. When the evanescent waves are included (see solid lines), the responses at both boundaries are significantly modified for the longitudinal and flexural energies. In the flexural energy densities, the RTM results including evanescent waves agree better with the TWM solutions. However, the torsional energy density and all power flow results barely change, even near the boundaries.

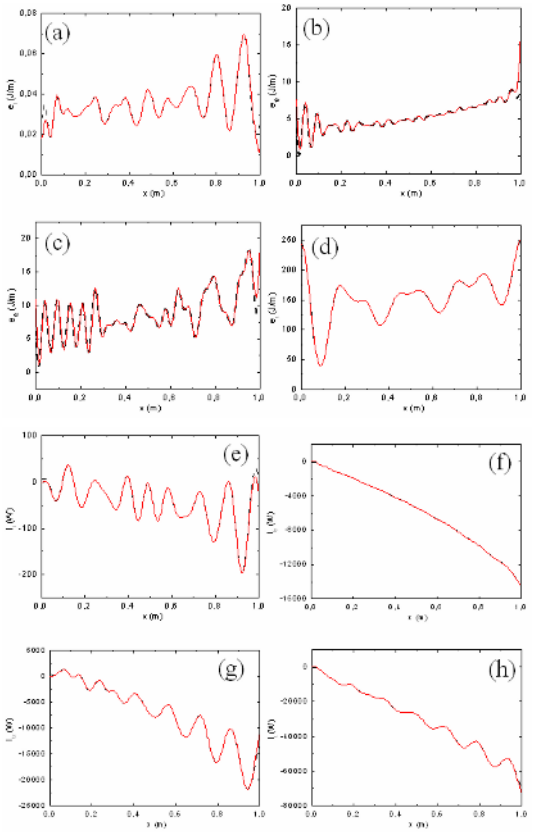

Fig. 7. Effects of evanescent wave on the spatial distribution of energy quantities (8 kHz octave band; η=0.05): (a) longitudinal energy density; (b) flexural energy density in y direction; (c) flexural energy density in z direction; (d) torsional energy density, (e) longitudinal energy power flow; (f) flexural power flow in y direction; (g) flexural power flow in z direction; (h) torsional power flow. ———, TWM; — — —, RTM considering phase, but neglecting evanescent wave.

Fig. 7 show spatial responses predicted by the modified RTM including the phase, but neglecting nearfield terms. Without the evanescent waves, the responses in the very vicinity to the boundaries slightly differ for longitudinal and flexural energy densities in Figs. 7(a)-(c). However, the predicted results for torsion and all the active power flows are rarely affected by the evanescent waves. As a conclusion, evanescent waves can be commonly neglected for high frequency energy prediction.

The effect of frequency on the spatial distribution of the flexural energy density was also investigated by changing the octave band from 125 Hz to 4 kHz, as shown in Fig. 8. One can clearly see that, as the frequency becomes higher, the RTM results agree

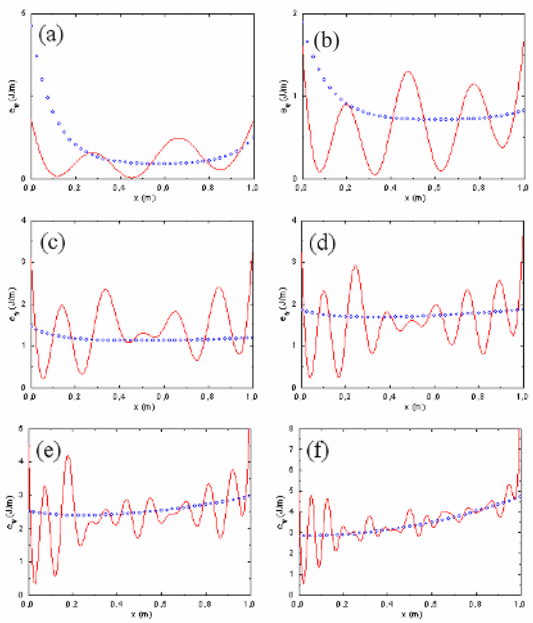

Fig. 8. Effects of frequency band on the spatial distribution of flexural energy density in y-direction (η=0.05). The center frequency f_c in each octave band is given by: (a) 125 Hz, (b) 250 Hz, (c) 500 Hz, (d) 1 kHz, (e) 2 kHz, (f) 4 kHz. ———, TWM; ○, conventional RTM.

better with the exact solutions; at high frequencies, local fluctuations are noticeably attenuated. Physibcally, at high frequencies a high overlap of many modes results in rather spatially smooth responses.

Effects of damping loss factor on the spatial response are shown in Fig. 9. In Fig. 9 (a), the vibration energy is fairly evenly distributed over the entire beam owing to small damping, although the local fluctuation is substantial. The RTM results are slightly overestimated from the mean value of the exact solution for small damping cases. As the damping increases, the vibration energy decreases sharply in space as the observation point goes farther away from the excitation point. These results clearly show the relation between the precision of the RTM and the internal damping of the structures.

In addition to the single curved beam, a connected, curved, two-beam structure in Fig. 10 was considered. Radii of curvature are R_1=0.25 m and R_2=1 m, in which the subscript *1* is for the left beam and *2* the beam in the right-hand side.

These beams are made of steel and the dimensions of the left beam were $b_1=1\times10^{-2}$ m, $h_1=1\times10^{-2}$ m, L_1=1 m, and the dimensions of the right beam were $b_2=2.5\times10^{-3}$ m, $h_2=2.5\times10^{-3}$ m, L_2=1 m. The excitation

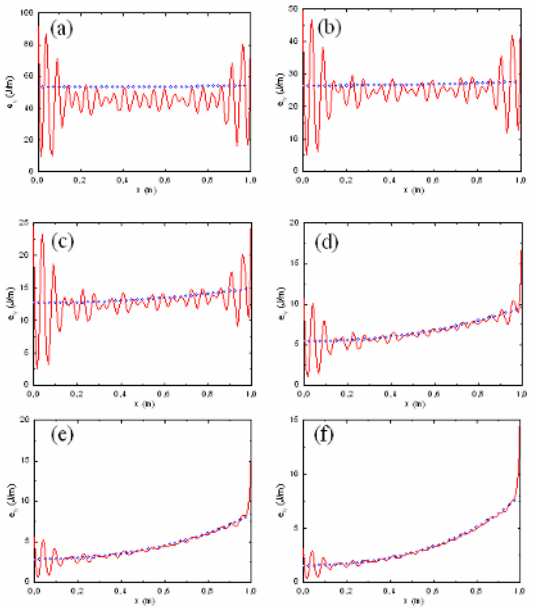

Fig. 9. Effects of damping on the spatial distribution of flexural energy density in y-direction (8 kHz octave band): (a) η=0.005, (b) η=0.01, (c) η=0.02, (d) η=0.04, (e) η=0.06, (f) η=0.08. ——, TWM; ○, conventional RTM.

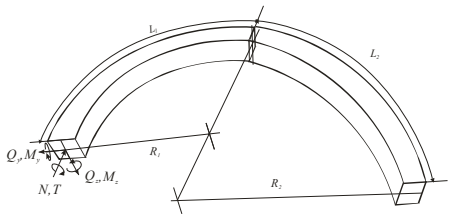

Fig. 10. A coordinate system of a connected beam structure.

condition was given at the left end of the whole structure, $\{N, Q_y, Q_z, M_y, M_z, T\} = \{1,1,1,1,1,1\}$

Fig. 11 shows a comparison between RTM and TWM at 8 kHz octave band with η_1=0.05 and η_2=0.01. Similar to the previous results, the band-averaged RTM results of the connected structure represent the overall trend without exhibiting local oscillations. Because the sectional areas and the radii of the curvature are different, abrupt changes at the junction were observed.

The decay rate of energy in the left beam is somewhat stiffer than that in the right beam, because the damping loss factor of the left beam is much larger than that of the right beam.

In Fig. 12, power reflection and transmission coefficients at the joint of the coupled beams are shown

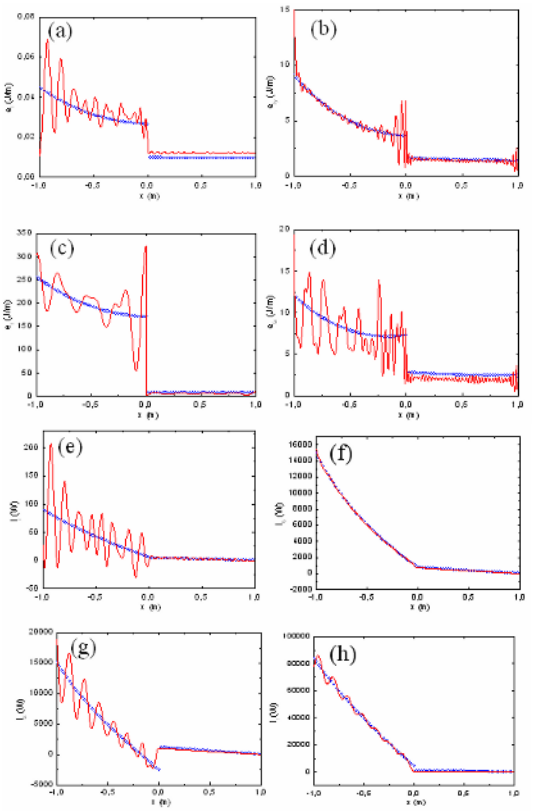

Fig. 11. Spatial distributions of energy quantities for a connected beam system excited at left end (8 kHz octave band, η_1=0.005, η_2=0.001): (a) longitudinal energy density; (b) flexural energy density in y direction; (c) flexural energy density in z direction; (d) torsional energy density, (e) longitudinal energy power flow; (f) flexural power flow in y direction; (g) flexural power flow in z direction; (h) torsional power flow. ——, TWM; ○, conventional RTM.

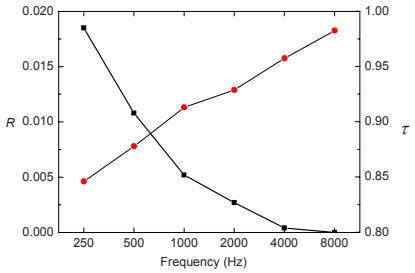

Fig. 12. Power reflection and transmission coefficients at the junction for an incident flexural wave. ——■——, Power reflection coefficient R; ——●——, power transmission coefficient τ.

when a flexural wave is incident on the joint. The power transmission coefficient goes high as the frequency increases, while the power reflection coeffi-

cient converges to zero. As the frequency becomes higher, the ratio between the radius of curvature and the wavelength increases. It gets easier for structural waves to transmit through the junction at high frequencies due to small impedance mismatch.

As discussed in Sec. 3.4, the MOF is a good indicator for validity of RTM. To examine the effect of MOF, we randomly selected 50 different cases by changing the length of the beam, the frequency of interest, and the damping loss factor. Ranges of variability for three parameters are follows: 0.005-0.05 for the loss factor, 1 kHz-8 kHz for the frequency, 0.5-1.5 m for the length of the beam structure. As a result of the parametric variations, the MOF have changed from 0.01 to 1. The relative error is defined as

$$\varepsilon = \frac{1}{n}\sum_{n}\left(\frac{y_{RTM} - y_{TWM}}{y_{RTM}}\right)_n, \tag{21}$$

where n denotes the number of the observation points used in the analysis of spatial distribution. In general, a denominator in the definition of a relative error should be the true value. However, when the true value becomes zero, the error gets infinite. Therefore, we adopted the RTM results as a reference value under the assumption that RTM solution represents the mean value in most cases. Fig. 13 displays the calculated relative error is as a function of the MOF. The regression curve using 50 scattered data can be obtained by using the first order exponential function as

$$\varepsilon = 15.3 \cdot \exp\left(-6.3 \cdot MOF\right), \tag{22}$$

which is drawn as the solid curve in the figure. Notwithstanding the fact that the variations are substantial in the low MOF range, one can conclude that the relative error is inversely proportional to the MOF.

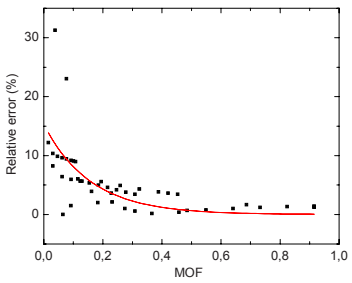

Fig. 13. Relative error as a function of MOF. ■, Collected data; ———, regression curve.

Reasonably small errors are found even below unity in MOF, being somewhat different from the finding by Fahy and Mohammed [29].

5. Conclusions

Spatial distributions of vibrational energies and energy flows of curved beams have been investigated based on the Euler-Bernoulli theory. Both the conventional and the modified ray tracing methods were applied to predict the vibrational energy considering mode conversions among longitudinal, flexural, and torsional waves. The modified RTM is able to include nearfield waves and phase information; therefore, a displacement or a velocity can be predicted as well as energy responses, while the conventional RTM can predict only a smoothly varying overall energy tendency without local fluctuations by neglecting the interference. Because fluctuations become smaller as the frequency and the structural damping go higher, the conventional RTM is sufficient for high overlap conditions. When evanescent waves were taken into account, the flexural energy responses were noticeably improved only in the very vicinity of boundaries. For a connected two-beam system having different radii and cross sectional areas, the conventional and modified RTM can properly simulate the wave transmission and reflection phenomena. By changing the frequency, the damping, and the length of the beam, the precision of the simulation was examined. The precision of the RTM increases with increasing MOF.

Acknowledgment

This work was partially supported by the BK21 Project.

References

[1] R. H. Lyon and R. G. DeJong, *Theory and application of statistical energy analysis*, Butterworth-Heinemann, Boston, USA, (1975).

[2] D. J. Nefske and S. H. Sung, Power flow finite element analysis of dynamic systems: basic theory and application to beams, *Trans. ASME, J. Vib. Acoust., Stress, and Reliability in Design* 111 (1) (1989) 94-100.

[3] J. C. Wohlever and R. J. Bernhard, Mechanical energy flow models of rods and beams, *J. Sound*

Vib. 153 (1) (1992) 1-19.

[4] R. S. Langley, On the vibrational conductivity approach to high frequency dynamics for two-dimensional structural components, *J. Sound Vib.* 182 (4) (1995) 637-657.

[5] A. L. Bot, M. N. Ichchou, and L. Jezequel, Energy flow analysis for curved beams, *J. Acoust. Soc. Am.* 102 (2) (1997) 943-954.

[6] M. R. Schroeder, Digital simulation of sound transmission in reverberant spaces, *J. Acoust. Soc. Am.* 47 (2) (1969) 424-431.

[7] A. Krokstad, S. Stroem and S. Soersdal, Calculating the acoustical room response by the use of a ray tracing technique, *J. Sound Vib.* 8 (1) (1968) 118-125.

[8] K.-S. Chae and J.-G. Ih, Prediction of vibrational energy distribution in the thin plate at high-frequency bands by using the ray tracing method, *J. Sound Vib.* 240 (2) (2001) 263-292.

[9] S. J. Walsh and R. G. White, Mobility of a semi-infinite beam with constant curvature, *J. Sound Vib.* 221 (5) (1999) 887-902.

[10] K. F. Graff, *Wave motion in elastic solids*, Clarendon Press, Oxford, UK, (1975).

[11] S.-K. Lee, B. R. Mace and M. J. Brennan, Wave propagation, reflection and transmission in curved beams, *J. Sound Vib.* 306 (3-5) (2007) 636-656.

[12] C. G. Culver, Natural frequencies of horizontally curved beams, *J. Struct. Div., Proc. ASCE* 93 (ST2) (1967) 189-203.

[13] C. P. Tan and S. Shore, Dynamic response of a horizontally curved bridge, *J. Struct. Div., Proc. ASCE* 94 (ST3) (1968) 761-781.

[14] C. H. Yoo and J. P. Fehrenbach, Natural frequencies of curved girders, *J. Eng. Mech., Proc. ASCE* 107 (2) (1981) 339-354.

[15]I . U. Ojalvo, Coupled twist-bending vibration of incomplete elastic rings, *Int. J. Mech. Sci.* 4 (1962) 53-72.

[16] A. S. Gendy, A. F. Saleeb and T. Y. P. Chang, Generalized thin-walled beam models for flexural-torsional analysis, *Comput. Struct.* 42 (4) (1992) 531-550.

[17] S. Shore and S. Chaudhuri, Free vibration of horizontally curved beams, *J. Struct. Div., Proc. ASCE* 98 (3) (1972) 793-796.

[18] J. Lee and S.-E. Kim, Flexural-torsional coupled vibration of thin-walled composite beams with channel sections, *Computers and Structures* 80 (2) (2002) 133-144.

[19] A. S. Gendy and A. F. Saleeb, Vibration analysis of coupled extensional/flexural/torsional modes of curved beams with arbitrary thin-walled sections, *J. Sound Vib.* 174 (2) (1994) 261-274.

[20] E. Reissner, A variational analysis of small finite deformations of pretwisted elastic beams, *Int. J. Solids Struct.* 21 (7) (1985) 773-779.

[21] A. E. Love, *A treatise on the mathematical theory of elasticity*, Dover Publications, New York, USA, (1944).

[22] L. S. D. Morley, Elastic waves in a naturally curved rod, *Q. J. Mech. Appl. Math.* 14 (2) (1961) 155-172.

[23] V. Z. Vlasov, *Thin walled elastic beams*, National Science Foundation, Washington D.C., USA, (1961).

[24] A. P. Dowling and J. E. Williams, *Sound and sources of sound*, Wiley and Sons, New York, USA, (1983).

[25] R. Gunda, S. M. Vijayakar and R. Singh, Method of images for the harmonic response of beams and rectangular plates, *J. Sound Vib.* 185 (5) (1995) 791-808.

[26] J. M. Parot and C. M. Thirard, Ray techniques for modeling vibratory fields, *Proc. of Euro-Noise 95*, Lyon, France. (1995) 453-456.

[27] C. Wu and B. Lundberg, Reflection and transmission of the energy of harmonic elastic waves in a bent bar, *J. Sound Vib.* 190 (4) (1996) 645-659.

[28] M. R. Schroeder and H. Kuttruff, On frequency response curves in rooms: comparison of experimental, theoretical, and Monte Carlo results for the average frequency spacing between maxima, *J. Acoust. Soc. Am.* 34 (1) (1962) 76~80.

[29] F. J. Fahy and A. D. Mohammed, A study of uncertainty in applications to coupled beam and plate systems, part I: computational experiments, *J. Sound Vib.* 158 (1) (1992) 45-67.

[30]I . Moens, D. Vandepitte and P. Sas, Wavelength criteria for the validity of the energy finite element method for high frequency vibrations, *Proc. of Seventeenth International Congress on Acoustics*, Rome, Italy. (2001) CD-Rom.

[31] C.-H. Jeong, J.-G. Ih and J. H. Rindel, An approximate treatment of reflection coefficient in the phased beam tracing method for the simulation of enclosed sound fields at medium frequencies, *Appl. Acoust.* 69 (7) (2008) 601-613.

[32] C.-H. Jeong and J.-G. Ih, A note on the proper frequency resolution for the room transfer function

in the phased beam tracing method, *Appl. Acoust.* 70 (1) (2009) 120-128.

Cheol-Ho Jeong received his M.S. and Ph.D. degrees from KAIST in 2002 and 2007, respectively. He is currently an assistant professor in the Department of Electrical Engineering at Technical University of Denmark in Denmark. His research interests include room acoustics, building acoustics, and structural acoustics.

Jeong-Guon Ih earned M.S. and Ph.D. degrees from KAIST in 1981 and 1985, respectively. He is currently a full professor in the Department of Mechanical Engineering at KAIST in Daejeon, Korea. He serves as an Editor of the Applied Acoustics journal and the head vice-president of the Acoustical Society of Korea. His research interests include duct acoustics, vehicle noise/vibration control, theoretical and experimental modeling of vibro-acoustic fields and sources, product sound quality.